Journal of Applied Mathematics and Physics, 2024, 12, 4030-4041
https://www.scirp.org/journal/jamp
ISSN Online: 2327-4379
ISSN Print: 2327-4352

Optimization Analysis of Sliding Electrical Contact Interface Based on Electromechanical Coupling

Pengfei Yue, Jiahe Ma, Ronghao Shi*, Kexing Song

Henan Key Laboratory of Advanced Conductor Materials, Institute of Materials, Henan Academy of Sciences, Zhengzhou, China
Email: *smartsrh@hnas.ac.cn

How to cite this paper: Yue, P.F., Ma, J.H., Shi, R.H. and Song, K.X. (2024) Optimization Analysis of Sliding Electrical Contact Interface Based on Electromechanical Coupling. *Journal of Applied Mathematics and Physics*, **12**, 4030-4041.
https://doi.org/10.4236/jamp.2024.1211246

Received: May 30, 2024
Accepted: November 26, 2024
Published: November 29, 2024

Abstract

This work addresses the critical issue of current density distribution in the sliding electrical contact interface based on electromechanical coupling, which is essential for minimizing damage and enhancing performance. Using electromechanical coupling analysis and finite element analysis (FEA), the effects of initial contact pressure, pulse current input, and armature speed on current density are examined. Key findings indicate that optimizing the convex rail and armature structures significantly reduces peak current density, improving uniformity and reducing damage. These optimizations enhance the efficiency, accuracy, and service life of sliding electrical contact interfaces, providing a theoretical foundation for designing more durable and efficient high-current-density applications.

Keywords

Sliding Contact Interface, Electromagnetic Propulsion, Current Density Distribution, Finite Element Analysis

1. Introduction

Electromagnetic launch systems (EMLs) utilize electromagnetic forces generated by high currents passing through the armature and rails to propel projectiles at high velocities, serving as a kinetic energy accelerator [1]. The extremely high initial launch velocity is driven by intense pulsed currents [2], which not only produce significant Joule heating but also expose the system to a transient, complex environment involving coupled electromagnetic, thermal, and mechanical fields [3]. This imposes stringent requirements on current-carrying capacity, posing significant challenges to the launch efficiency, accuracy, and operational lifespan of

EML systems [4].

The contact performance between the rail and the armature is a critical factor in determining the launch efficiency of EML systems. Maintaining reliable sliding electrical contact under extreme multi-physics field conditions is inherently difficult [5]. During high-speed armature motion, current flow at the sliding contact interface exhibits the velocity skin effect (VSE) [6], characterized by highly localized current concentration at the contact interface. This leads to excessive peak current densities, which cause issues such as thermal loss [7], electromagnetic interference [8] [9], material degradation [10], and physical damage [11] [12].

VSE is unavoidable in the high-speed relative motion between the armature and the rail and plays a decisive role in the current density distribution at the electrical contact interface [13]. To effectively mitigate VSE, reduce peak current density at the contact interface, and minimize the thermal effects on the EML system, various approaches have been proposed. These strategies primarily fall into two categories: structural optimization [14] [15] and material design [16] [17]. Structural optimization, due to its shorter research cycles and relatively lower computational requirements, has gained particular attention. Studies have demonstrated that convex-shaped rails, at equivalent rail heights, can effectively increase the contact area and suppress VSE during high-speed armature motion [18]. However, convex rail designs are predominantly elliptical, and it remains unclear whether elliptical structures represent the optimal configuration for mitigating VSE during high-speed EML operation. Additionally, finite element analysis (FEA) of EML systems, involving complex multiphysics fields, demands substantial computational power and resources [19]. Therefore, it is imperative to identify convex rail structures capable of effectively suppressing VSE while minimizing computational resource usage.

This study introduces a VSE-based equivalent simplification analysis for three convex rail models. Finite element numerical simulations are employed to compare the effects of these rail structures on the trailing current density distribution at the electrical contact interface of EML systems. The objective is to identify the optimal convex rail structure for mitigating VSE. The proposed method and conclusions are further validated through a transient three-dimensional multi-physics launch model.

2. Model Construction

A foundational EML model is established, consisting of two parallel flat rails and a C-shaped armature, as illustrated in **Figure 1**. The rail and armature materials are copper and aluminum, respectively, with material properties listed in **Table 1**.

Based on the flat rail model, three convex rail designs—elliptical, trapezoidal, and rectangular—are constructed, each with a protrusion height fixed at 10 mm, as shown in **Figures 3(a)-(c)**. The armature structure adapts to the rail configuration, with the modifications highlighted in gray in **Figures 3(d)-(f)**. The material properties of the EML system remain unchanged.

Table 1. Parameters of materials.

	Conductivity σ/(S/m)	Density ρ_m/(kg/m^3)	Relative dielectric constant ε_r/1	Thermal conductivity κ/(W/m·K)
Copper rails	5.998×10^7	8940	1	400
Aluminum armature	3.774×10^7	2700	1	238

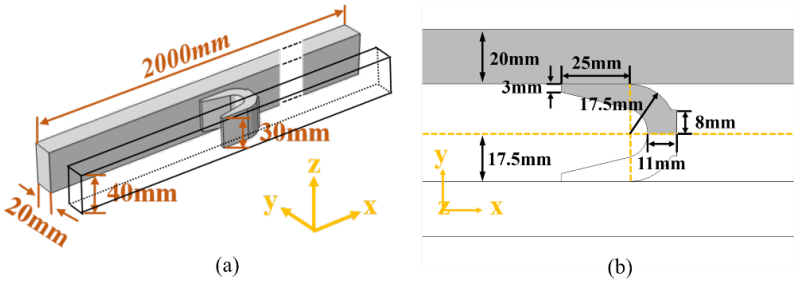

Figure 1. Model and Geometry of EML.

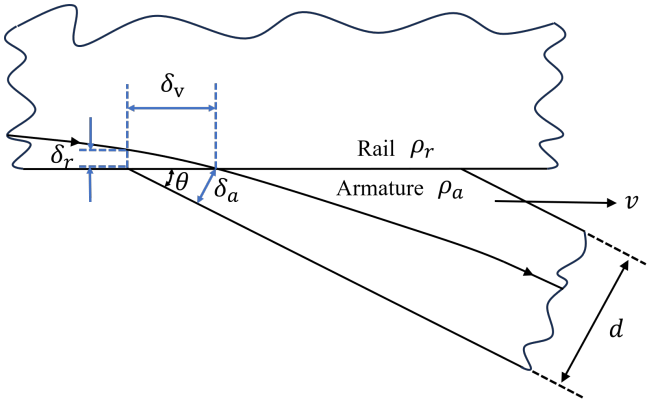

Figure 2. Current flow path of electrical contact interface under VSE.

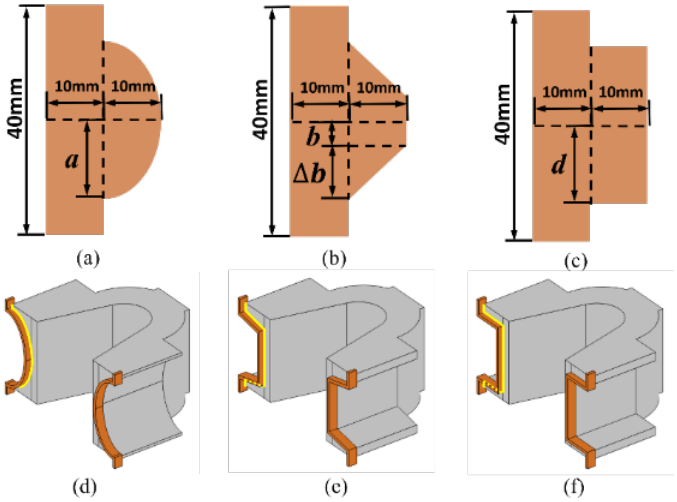

Figure 3. Geometric parameters and simplified model of convex guide rails: (a) elliptical guide rail; (b) trapezoidal guide rail; (c) rectangular guide rail.

Both the rails and armature are assumed to be non-ferromagnetic and isotropic, with electrical conductivity independent of temperature. The electromagnetic field within the EML system is described using the magnetic diffusion equation and current continuity equation in a moving coordinate system. Using vector potential and scalar potential as variables, the governing equations for the electromagnetic field are expressed as follows [20]:

$$\nabla^2 A - \sigma\mu\left(\frac{\mathrm{d}A}{\mathrm{d}t} + \nabla\phi\right) = 0 \tag{1}$$

$$\nabla\cdot\left(-\sigma\frac{\mathrm{d}A}{\mathrm{d}t} - \sigma\nabla\phi\right) = 0 \tag{2}$$

where σ is the electrical conductivity and μ is the magnetic permeability. Assuming ideal contact between the armature and the rails (no contact resistance), the relationship between the VSE skin depth and the armature speed is shown in **Figure 2**. The skin depth is calculated as [21]:

$$\delta_v = \frac{\rho_a^2}{\mu_0\rho_r v\theta^2} \tag{3}$$

where δ_v is the VSE skin depth, and ρ_a, ρ_r represents the electrical resistivities of the armature and rail materials, respectively.

Using this theory, the rail structures in the simplified model are modified. To enhance model convergence, the skin depth corresponding to VSE is set, from which the armature velocity is calculated using Equation (3). Since current is concentrated on the rail surface near the trailing edge of the armature, all three convex rail designs are simplified to a width of 3 mm and a thickness of 1 mm, with a 1 mm contact width between the armature and the rail. **Figures 3(d)-(f)** depict the three-dimensional simplified EML models at the calculated armature velocity, where the orange regions represent the simplified rails and the yellow lines indicate the trailing contact interface between the rail and armature.

In each of the three finite element (FE) simplified models, a terminal current of 700 kA is applied to one end of the rail, with the same side grounded at the other end to form a closed circuit. To systematically analyze the impact of different convex rail designs on mitigating VSE, a parametric study of line current density distribution at the trailing contact interface is conducted for the three simplified models. The optimal structural parameters for each convex rail design are identified and compared against the flat rail configuration. Finally, a three-dimensional transient electromagnetic-thermal coupled FE model is established to validate the reliability of the study.

3. Calculation and Analysis

The variation of current density J at the trailing edge of the contact interface with structural parameters of the simplified convex rails is shown in **Figure 4**.

Elliptical Rail: **Figure 4(a)** illustrates that as the semi-axis a of the elliptical rail increases, the trailing arc length of the contact interface decreases, and the current

density concentration shifts from the center toward the ends, leading to a more uniform distribution. The peak current density $J_{\max}$ decreases accordingly. The structure is optimal when $a = 14$ mm for a rail protrusion height of 10 mm.

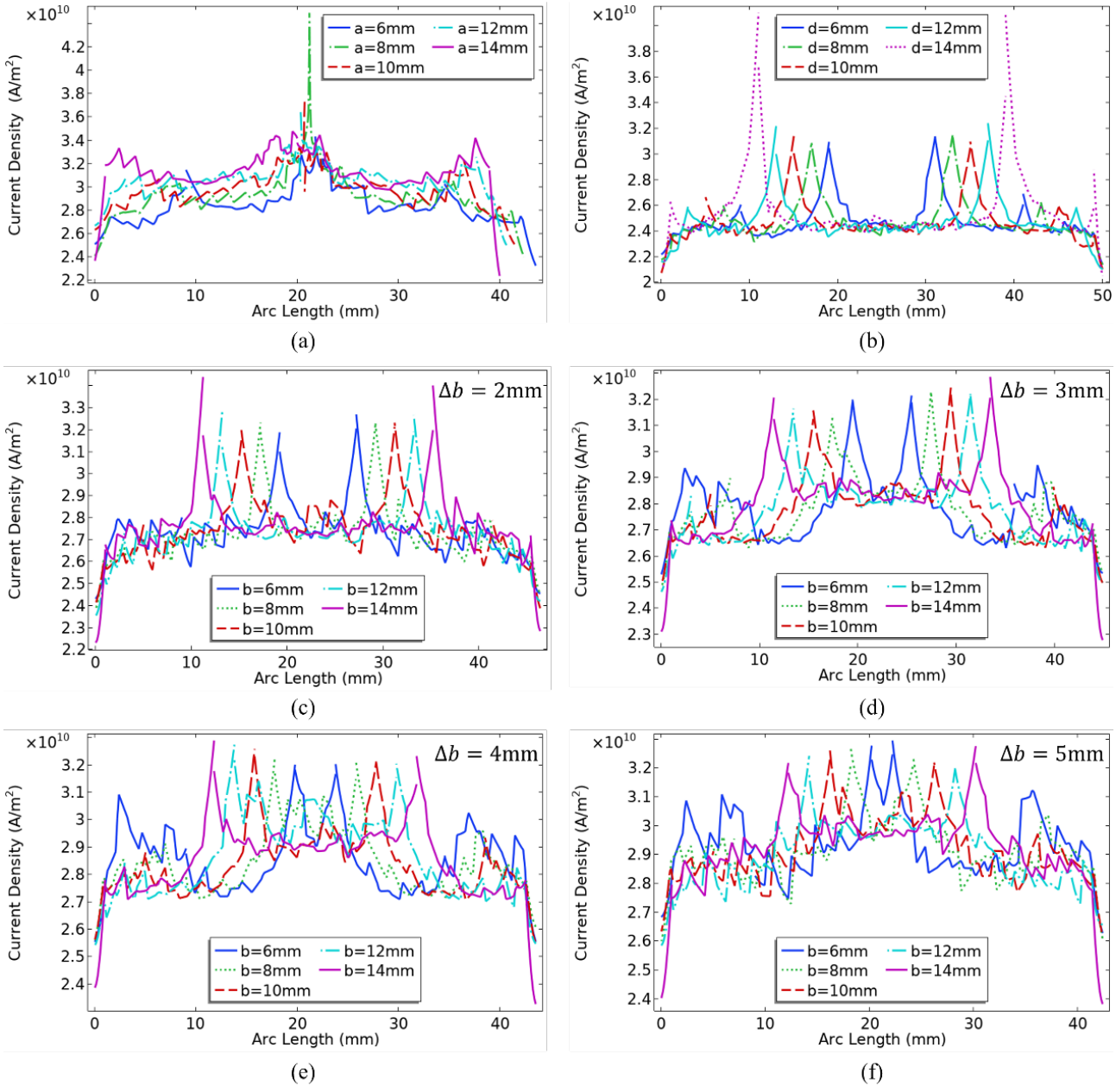

Figure 4. The relationship between J(A/m^2) and the structural parameters for the elliptical, trapezoidal, and rectangular rails.

Rectangular Rail: Figure 4(b) shows two prominent current density concentration points at the trailing edge of the rectangular rail's contact interface. As d, the width of the rail, increases, these concentration points shift outward. The minimum $J_{\max}$ occurs when $d = 12$ mm, indicating the optimal structure.

Trapezoidal Rail: **Figures 4(c)-(f)** depict the current density distribution at

the trailing edge for different short side dimensions b and height variations $\Delta b = 2$ mm, $\Delta b = 3$ mm, $\Delta b = 4$ mm, $\Delta b = 5$ mm. At $\Delta b = 2$ mm, two distinct J concentration points are observed. For $3\text{ mm} \le \Delta d \le 5\text{ mm}$, four concentration points appear (two at the center and two at the ends). The optimal structure occurs at $\Delta b = 2$ mm, $b = 10$ mm, where $J_{\max}$ is minimized.

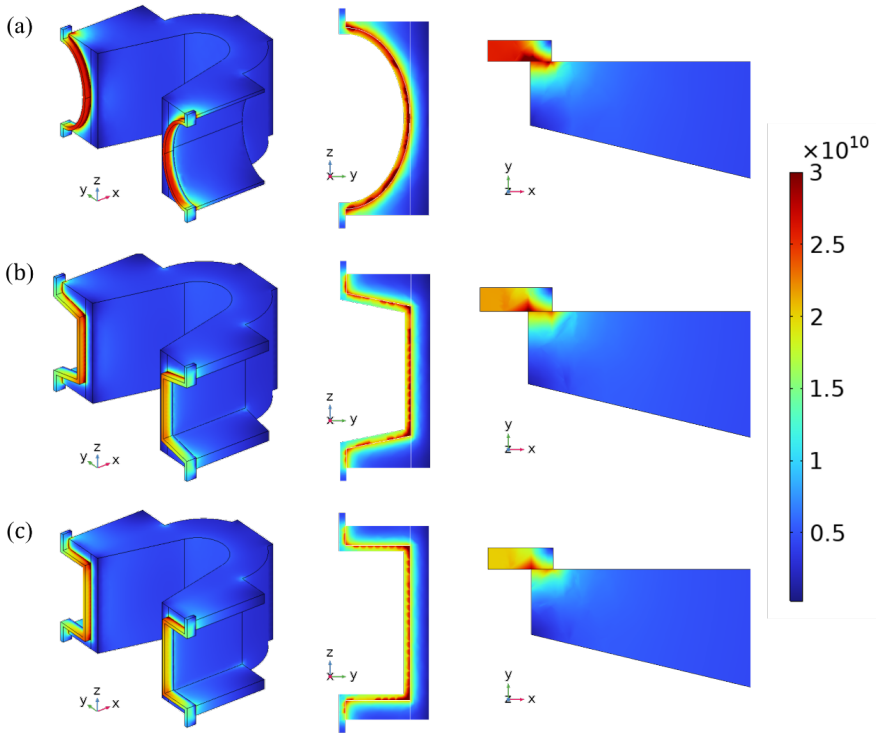

Figure 5. The current density distributions for the three optimal convex rail structures. The first column presents 3D distributions. The second column shows the *y*-*z* sectional views at the trailing contact interface. The third column provides *x*-*y* sectional views at the central position of the armature.

Under the optimal configurations of the three simplified convex rails, the current density distributions for the EML system are shown in **Figure 5**. **Figures 5(a)-(c)** illustrate the results for elliptical, trapezoidal, and rectangular rails, respectively. The comparison of **Figures 5(a)-(c)** reveals that the elliptical rail exhibits more pronounced concentration across the contact interface. In contrast, the trapezoidal and rectangular rails show J concentration localized at the tips of the rail protrusions. These concentration points align with the calculated results in **Figure 4**, further validating the structural analysis. The third column of **Figure 5** confirms that the simplified model effectively captures the current concentration phenomenon induced by VSE during high-speed armature motion, providing reliable insights into the electromagnetic behavior of EML systems.

The comparison of the current density distributions along the arc length at the trailing edge of the contact interface for the three simplified convex rail models and the flat rail model is shown in **Figure 6**.

The results reveal that the flat rail exhibits relatively high overall current density, with multiple small peaks and troughs distributed across the arc length. In contrast, convex rails show more pronounced current density concentration points, with the rectangular convex rail having the most prominent peaks.

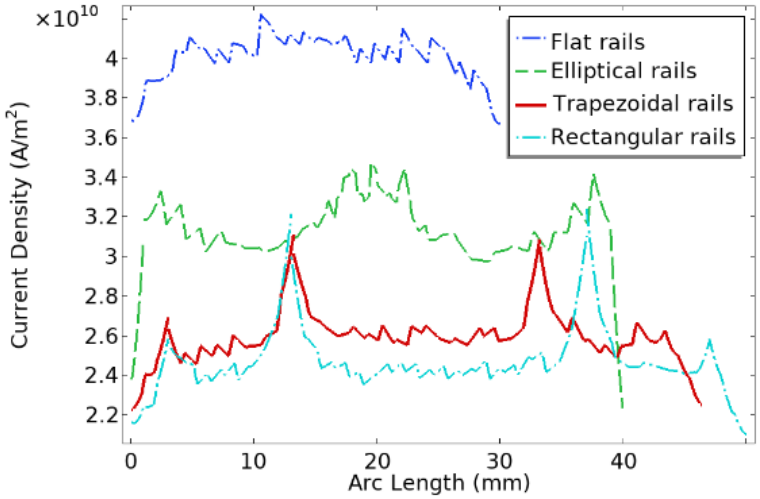

Figure 6. Comparison of current density J (A/m^2) at the trailing edge for optimal simplified convex rails and flat rail.

Convex rails demonstrate significant advantages over flat rails in mitigating VSE, with the trapezoidal rail showing the most favorable performance among the convex designs. However, notable JJJ concentration points persist at the tips of the rail protrusions, suggesting that further structural refinements may be needed to address these localized concentrations effectively.

4. 3D Transient Analysis

Based on the preceding analysis, 3D finite element analysis (FEA) models were developed for the optimal structural parameters of the three convex rails (elliptical, trapezoidal, and rectangular). The models incorporate transient coupling between the electromagnetic and thermal fields. The electromagnetic force F acting on the armature is governed by [22]:

$$F = \frac{1}{2} L_r' i^2 \tag{4}$$

where L_r' is the inductance gradient, assumed constant with a value of $L_r' = 0.4\ \mu\text{H/m}$, i is the input pulsed current with a waveform as shown in **Figure 7**, peaking at 700 .

The coupled electromagnetic-thermal model for the EML system incorporates the temperature field control equation [23]:

$$c\rho_m \frac{\partial T}{\partial t} = \nabla \cdot (\kappa \nabla T) + \frac{J^2}{\sigma} + \mu_f F_N v \tag{5}$$

where T is the material temperature, μ_f is the sliding friction coefficient at the

contact interface, F_N is the contact interface pressure, and $v = 300$ m/s is the armature velocity. Given the dry sliding conditions at the interface during high-speed motion [24], the friction coefficient is set to $\mu_f = 0.15$ [25]. To ensure reliable electrical contact, the contact pressure is determined as 80 MPa based on Marshall's "1 g/A" guideline [26] and conforms to the Copper-Mikic-Yovanovich theory [27].

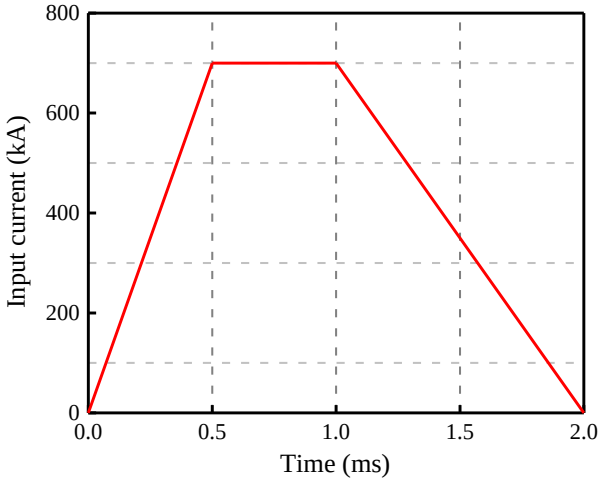

Figure 7. Input pulsed current with the waveform.

The 3D finite element transient electromagnetic-thermal coupling analysis is shown in **Figure 8**. After 1.3 ms of current application in the EML, the launch velocity and displacement of the armature under flat rails and three convex rail designs are presented in **Figure 8(a)**. The figure indicates that the armature's launch velocity and displacement for convex rails are slightly compromised compared to the flat rail. This is due to the increased mass of the armature paired with convex rails compared to that paired with the flat rail.

Figure 8(b) illustrates the peak temperature $T_{\max}$ at the sliding contact interface at the final time, which rises due to the combined effects of Joule heating and frictional heating. It indicates that frictional heating is the dominant factor influencing thermal effects at the final moment. Compared to the flat rail, the trapezoidal rail exhibits nearly unchanged Joule heating, while the elliptical and rectangular rails show increased Joule heating. However, all convex rails generate less frictional heating than the flat rail. Overall, the trapezoidal rail demonstrates the best thermal performance at the contact interface. **Figure 8(c)** shows the peak current density $J_{\max}$. and peak temperature $T_{\max}$ of the armature for different rail designs at the final moment of EML launch. The elliptical rail exhibits a significant increase in $J_{\max}$ compared to the results in **Figure 8(b)**. All convex rails exhibit slight increases in $T_{\max}$. In contrast, **Figure 8(d)** presents the average current density J_{ave} and average temperature T_{ave} of the armature for different rail designs at the final moment. The values for convex rails are reduced compared to the flat rail.

Compared to the flat rail, convex rails result in increases in J_{max} and T_{max} of

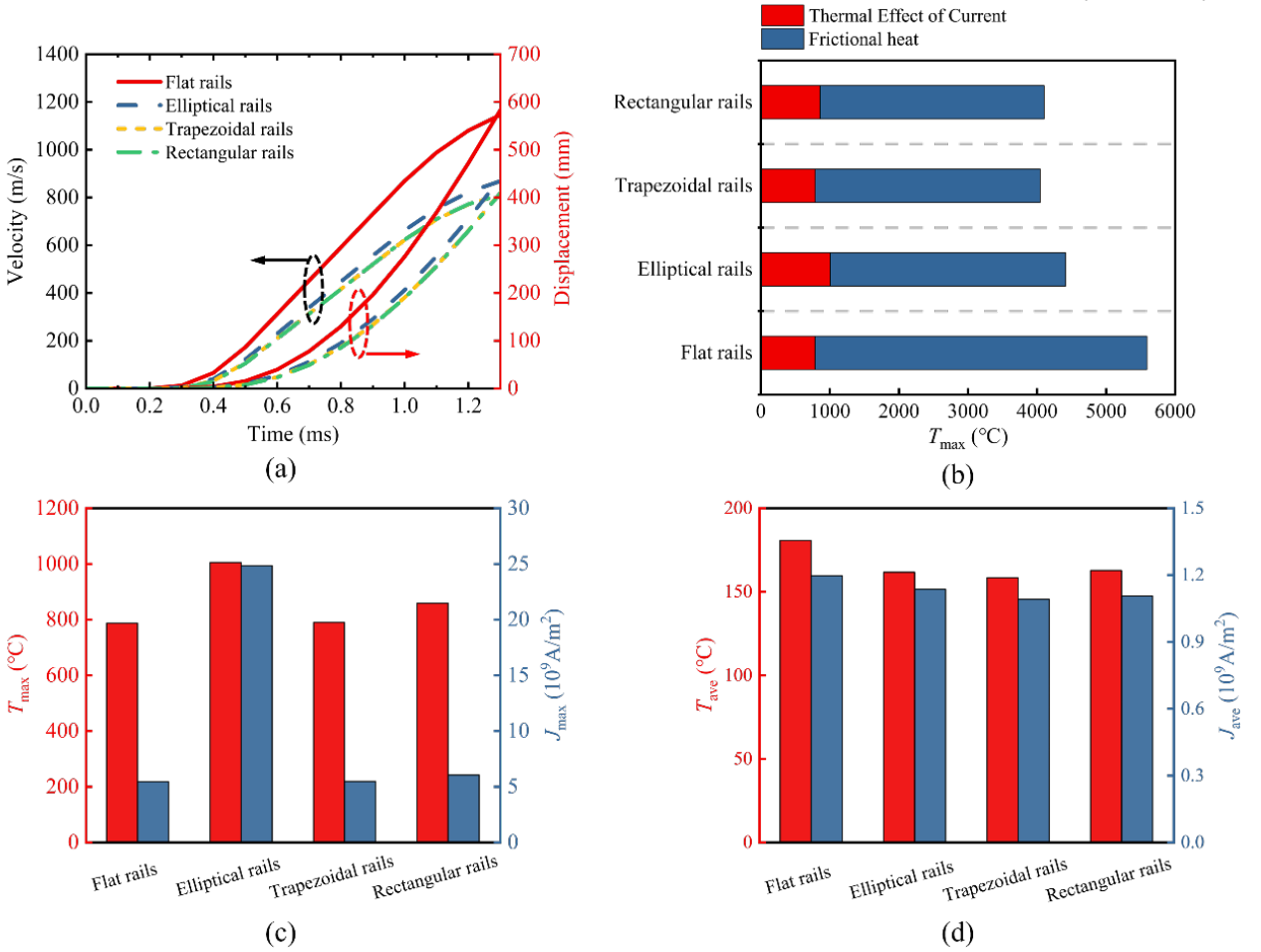

Figure 8. Input pulsed current with the waveform.

the armature, with the elliptical rail showing the highest J_{max}. However, these increases do not lead to excessive growth in T_{max}, J_{ave}, or T_{ave}. Convex rails demonstrate significant advantages in suppressing the velocity skin effect (VSE) and reducing the thermal effects in the launch system. Among the convex rails, the trapezoidal rail performs the best, indicating that it has greater advantages in mitigating VSE and reducing thermal effects compared to the elliptical and rectangular designs.

5. Conclusions

This study proposed a 3D finite element model of rail structures based on the velocity skin effect (VSE) theory, employing equivalent simplification. By comparing the peak current density at the trailing edge of the contact interface for three convex rail designs (elliptical, trapezoidal, and rectangular), the effectiveness of convex rails in suppressing VSE was analyzed. The findings were validated through calculations and analysis using a 3D transient electromagnetic-thermal coupling model of the EML system. The key conclusions are as follows:

1) The 3D finite element model of rail structures, simplified based on VSE theory, effectively reduces computational resources and saves computation time compared to conventional 3D transient studies.

2) Convex rails demonstrate significant advantages in suppressing the VSE at the contact interface of the EML launch system and in reducing thermal effects. Among the designs, the trapezoidal rail outperforms both the elliptical and rectangular rails.

3) The impact of armature structure and geometric parameters on the current density distribution at the sliding contact interface of the EML system should also be considered in the structural optimization of EML systems.

Acknowledgements

This research was funded by the Henan Academy of Sciences under the Start-up Project Funding (Project No. 242017001), and the Scientific and Technological Research Project (Project No. 242217018).

Conflicts of Interest

The authors declare no conflicts of interest regarding the publication of this paper.

References

[1] Mao, W., Pang, T., Guo, Z., Bai, H., Huang, Z. and Jin, X. (2024) Analysis of the Research Progress of Electromagnetic Railgun Based on CiteSpace. *IEEE Access*, **12**, 3499-3513. https://doi.org/10.1109/access.2023.3349028

[2] Gallo, F., Satapathy, S. and Ravi-Chandar, K. (2009) Melting and Cavity Growth in the Vicinity of Crack Tips Subjected to Short-Duration Current Pulses. *IEEE Transactions on Magnetics*, **45**, 584-586. https://doi.org/10.1109/tmag.2008.2008572

[3] Fan, C., Xu, S., Du, J., Chen, D. and Cheng, L. (2023) Research Progress in Current-Carrying Friction and Wear of Silver-Based Electrical Contact Materials. *Materials Research and Application*, **17**, 495-502.

[4] Li, S., Li, J., Xia, S., Zhang, Q. and Liu, P. (2019) Phase Division and Critical Point Definition of Electromagnetic Railgun Sliding Contact State. *IEEE Transactions on Plasma Science*, **47**, 2399-2403. https://doi.org/10.1109/tps.2019.2891175

[5] Chemerys, V.T. (2013) Key Problems of Railgun: New Concept for Their Resolution. *Procedia Engineering*, **58**, 377-383. https://doi.org/10.1016/j.proeng.2013.05.043

[6] Engel, T.G., Neri, J.M. and Veracka, M.J. (2008) Characterization of the Velocity Skin Effect in the Surface Layer of a Railgun Sliding Contact. *IEEE Transactions on Magnetics*, **44**, 1837-1844. https://doi.org/10.1109/tmag.2008.922310

[7] Zhou, P. and Li, B. (2021) Exergy Analysis of the Electromagnetic Railgun. *IEEE Transactions on Plasma Science*, **49**, 3980-3987. https://doi.org/10.1109/tps.2021.3124314

[8] Gharib, L. and Keshtkar, A. (2019) Electromagnetic Interference of Railgun and Its Effect on Surrounding Electronics. *IEEE Transactions on Plasma Science*, **47**, 4196-4202. https://doi.org/10.1109/tps.2019.2923061

[9] Chung, S.S.M. and Chuang, Y. (2016) Characteristics of Electromagnetic Radiation of a Railgun at the Final Firing Stage. *IEEE Transactions on Plasma Science*, **44**, 49-

59. https://doi.org/10.1109/tps.2015.2502268

[10] Muzel, S.D., Bonhin, E.P., Guimaraes, N.M. and Guidi, E.S. (2020) Application of the Finite Element Method in the Analysis of Composite Materials: A Review. *Polymers*, **12**, Article 818.

[11] Zhu, Q., Dai, L., Liang, Z., Feng, Y. and Lin, F. (2022) Numerical Calculation Model and Efficiency Analysis of Distributed-Energy-Store Railgun. *IEEE Transactions on Plasma Science*, **50**, 3341-3350. https://doi.org/10.1109/tps.2022.3160486

[12] Bansal, D.G. and Streator, J.L. (2009) Behavior of Copper-Aluminum Tribological Pair under High Current Densities. *IEEE Transactions on Magnetics*, **45**, 244-249. https://doi.org/10.1109/tmag.2008.2008684

[13] Dai, K., Yang, Y., Yin, Q. and Zhang, H. (2019) Theoretical Model and Analysis on the Locally Concentrated Current and Heat during Electromagnetic Propulsion. *IEEE Access*, **7**, 164856-164866. https://doi.org/10.1109/access.2019.2952981

[14] Shvetsov, G.A. and Stankevich, S.V. (2011) Three-Dimensional Numerical Simulation of the Joule Heating of Various Shapes of Armatures in Railguns. *IEEE Transactions on Plasma Science*, **39**, 456-460. https://doi.org/10.1109/tps.2010.2087333

[15] Liu, Y., Guo, W., Zhang, T., Su, Z., Fan, W. and Zhang, H. (2019) Influence of Contacting Schemes on Electromagnetic Force and Current Density Distribution in Armature. *IEEE Transactions on Plasma Science*, **47**, 2726-2735. https://doi.org/10.1109/tps.2019.2907928

[16] Chemerys, V. (2014) Multilayer Structure of Electrical Conductivity for Contact Surface of Railgun. 2014 *IEEE International Power Modulator and High Voltage Conference* (*IPMHVC*), Santa Fe, 1-5 June 2014, 316-321. https://doi.org/10.1109/ipmhvc.2014.7287272

[17] Zhou, P. and Li, B. (2021) Numerical Calculation of Magnetic-Thermal Coupling and Optimization Analysis for Velocity Skin Effect. *IEEE Transactions on Plasma Science*, **49**, 3994-4001. https://doi.org/10.1109/tps.2021.3123821

[18] Lv, Q.A., Xiang, H.J., Lei, B., Zhang, Q., Zhao, K.Y., Li, Z.Y., *et al.* (2015) Physical Principle and Relevant Restraining Methods about Velocity Skin Effect. *IEEE Transactions on Plasma Science*, **43**, 1523-1530. https://doi.org/10.1109/tps.2015.2399952

[19] Aulisa, E., Capodaglio, G., Chierici, A. and D'Elia, M. (2021) Efficient Quadrature Rules for Finite Element Discretizations of Nonlocal Equations. *Numerical Methods for Partial Differential Equations*, **38**, 1767-1793. https://doi.org/10.1002/num.22833

[20] Lin, Q. and Li, B. (2016) Numerical Simulation of Interior Ballistic Process of Railgun Based on the Multi-Field Coupled Model. *Defence Technology*, **12**, 101-105. https://doi.org/10.1016/j.dt.2015.12.008

[21] Barber, J.P. and Dreizin, Y.A. (1995) Model of Contact Transitioning with "Realistic" Armature-Rail Interface. *IEEE Transactions on Magnetics*, **31**, 96-100. https://doi.org/10.1109/20.364721

[22] Li, H., Zhang, T., Chen, Y., An, Y., Hu, Y. and Jiao, C. (2019) Feasibility Study of a Repetitive Inductive Pulsed Power Supply Circuit for Electromagnetic Rail-Guns. *IEEE Transactions on Applied Superconductivity*, **29**, 1-6. https://doi.org/10.1109/tasc.2018.2882019

[23] Zhang, B., Kou, Y., Jin, K. and Zheng, X. (2021) A Multi-Field Coupling Model for the Magnetic-Thermal-Structural Analysis in the Electromagnetic Rail Launch. *Journal of Magnetism and Magnetic Materials*, **519**, Article ID: 167495. https://doi.org/10.1016/j.jmmm.2020.167495

[24] Li, C. and Xia, S. (2020) Study on Lubrication Characteristics of Metal Liquid Film Based on Electromagnetic-Elastic Mechanics-Hydrodynamics Multiphysics Coupling Model. *Materials*, **13**, Article 1056. https://doi.org/10.3390/ma13051056

[25] Zhu, C. and Li, B. (2020) Analysis of Sliding Electric Contact Characteristics in Augmented Railgun Based on the Combination of Contact Resistance and Sliding Friction Coefficient. *Defence Technology*, **16**, 747-752. https://doi.org/10.1016/j.dt.2019.12.007

[26] Xia, S., He, J., Chen, L., Xiao, Z. and Li, J. (2011) Studies on Interference Fit between Armature and Rails in Railguns. *IEEE Transactions on Plasma Science*, **39**, 186-191. https://doi.org/10.1109/tps.2010.2057452

[27] Ma, J., Shi, R., Han, D., Yue, P. and Song, K. (2024) Finite Element Analysis of Current Density Distribution in the Sliding Contact Interface of Electromagnetic Railguns: A Literature Review. *IEEE Access*, **12**, 84088-84109. https://doi.org/10.1109/access.2024.3414648